Eurographics Symposium on Rendering (2023)
T. Ritschel and A. Weidlich (Editors)

A Microfacet Model for Specular Fluorescent Surfaces and Fluorescent Volume Rendering using Quantum Dots

A. Benamira and S. Pattanaik

University of Central Florida

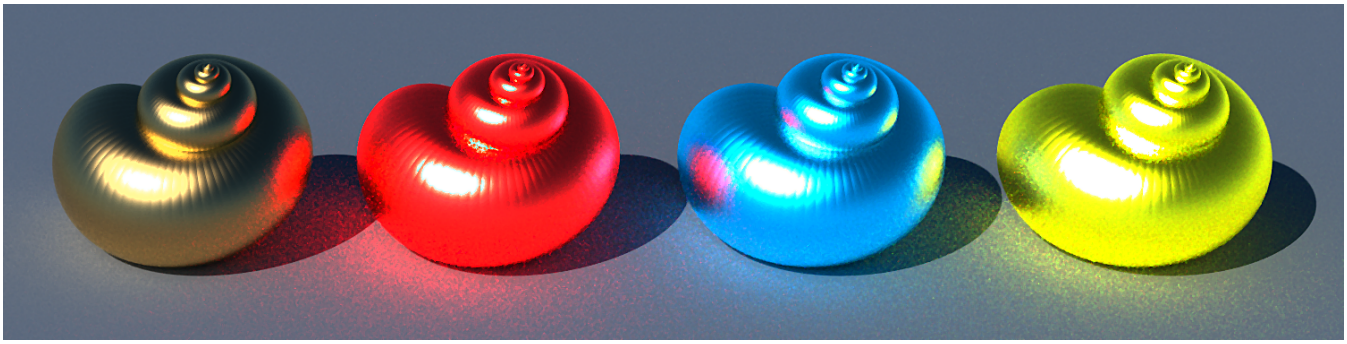

Figure 1: *Illustration of our fluorescent specular microfacet surface model. The farthest on the left is a gold snail shell object. The other three objects are coated with QDs which result in fluorescence. The parameters of the QD coatings are Radius: $\mathcal{R} = 5$ nm (red) $\mathcal{R} = 2$ nm (blue) and $\mathcal{R} = 3$ nm (green), Quantum Yield: $Q = 0.8$, Standard Deviation : $\delta_\lambda = 15$ nm and Density : $\rho = 0.5$.*

Abstract

Fluorescent appearance of materials results from a complex light-material interaction phenomenon. The modeling of fluorescent material for rendering has only been addressed through measurement or for simple diffuse reflections, thus limiting the range of possible representable appearances. In this work, we introduce and model a fluorescent nanoparticle called a Quantum Dot (QD) for rendering. Our modeling of the Quantum Dots serves as a foundation to support two physically based rendering applications. First a fluorescent volumetric scattering model and second, the definition of a fluorescent specular microfacet scattering model. For the latter, we model the Fresnel energy reflection coefficient of a QD coated microfacet assuming specular fluorescence, thus making our approach easily integrable with any microfacet reflection model.

CCS Concepts

• ***Computing methodologies*** → ***Reflectance modeling;***

1. Introduction

Light-matter interaction is a complex phenomenon that can yield a wide range of material appearances. Fluorescence is one such phenomenon. Simply put, an incident photon is absorbed by a molecule, one of the valence electrons of the molecule's electronic cloud is promoted to a higher energy state. The release of this absorbed energy can take multiple forms. One of them, called photoluminescence, is a radiative process where a photon is emitted by the molecule at a different - usually longer - wavelength. When the electron keeps the same spin, the phenomenon, named fluorescence, occurs nanoseconds after the absorption. So far, renderings of fluorescence are restricted to measured models [HHA*10] or diffuse reflection models [WWLP06, JHMD18]. We propose to reduce this restriction by introducing a microfacet based fluorescence model.

In this work, we first strive to establish a physically based rendering framework to render Quantum Dots (QDs). QDs are semiconductor nanoparticles that possess strong fluorescent properties, namely a high absorption in the Ultraviolet (UV) range and a high Quantum Yield (QY) i.e. a high conversion rate between absorbed and reemitted photons, and a narrow emission spectrum. QDs are the underlying basis for many applications like light-

DOI: 10.2312/sr.20231121

emitting diodes, biological cell marking and tracking or solar panel coating and are under intensive research effort [YTC*23, CLZ*23]. The unique properties of those nanocrystals derive from their nanometer-scale radius and call upon quantum physics laws of light-material interaction for rendering materials containing QDs.

Our QD framework supports two applications. First is the definition of an absorption and an emission spectrum for fluorescent volumetric rendering. Second, that we believe to be the strongest contribution of this paper, is the derivation of a fluorescent microfacet specular scattering model. Indeed, microfacet models are widely used to render specular surfaces. Nonetheless, to date, no model has been derived to simulate fluorescent specular reflection. To render specular fluorescence with our QD model, we simulate the behavior of the surface when sparsely coated with QDs. This coating is modeled as a monolayer of QDs placed on top of the surface. More precisely, we consider how this thin film modifies the Fresnel coefficients of the underlying surface and results in fluorescence. This leads to a new Bispectral Bidirectional Reflection and Reradiation Distribution Function (BBRRDF) for rough specular fluorescent surfaces. We can underline here that considering specular fluorescence is a simplifying assumption of the QD fluorescence behavior. This new analytical BBRRDF has adjustable physical parameters to control fluorescence appearance. We study the correctness of our model, validate it with available measured data, evaluate the influence of its parameters and demonstrate its application for rendering fluorescent volumes and material surfaces.

The contribution of our work is threefold:

- A rendering model for QDs nanoparticles.
- An analytical, physically based, absorption and emission function for fluorescent volume rendering.
- An analytical, physically based, BBRRDF for microfacet scattering models.

The paper is organized as follows. First we offer an overview of the state of the art in fluorescent material rendering, QD physics, and thin film surface coating rendering. Then, we lay out the theoretical background on which our work is based. Afterward, we describe our QD model for fluorescent volume rendering followed by the derivation of our BBRRDF model for fluorescent specular microfacet rendering. Finally, we investigate the validity of our model, we study the influence of the parameters on our model and demonstrate its applicability to rendering.

2. Previous Work

Photoluminescence When an object absorbs an electromagnetic wave it reaches a state of higher energy. One of the ways it can discharge that extra energy is by radiating light. If the discharge occurs immediately after the excitation, with no change in the spin of the electrons, then this phenomenon is called fluorescence [Lak06]. Most of the time, the emitted radiation is of lower energy than the absorbed one. The wavelength shift between the highest intensity of the absorption and emission spectrum is called the Stokes shift. The rare event of higher emitted energy compared to the absorbed energy corresponding to the Anti-Stokes shift is not addressed here.

As described below, fluorescent rendering is a complex problem that has been approached in two different ways. The first is the modeling of the reflection of fluorescent surfaces, which is the scope of the present work. The second, focuses on finding solutions to integrate fluorescent materials into a rendering algorithm.

Fluorescent materials. There have been two ways to characterize the fluorescence of a surface. One is by defining an emission and an absorption spectrum [JHMD18], the other uses a re-radiation matrix [HFW21]. This re-radiation matrix expresses how much light is converted from the input to the output wavelength for each input output wavelength configuration. Some works have focused on measuring [HHA*10] and compressing [HFW21, HTFW22] this re-radiation matrix which has the drawback of presenting a high memory overhead. In a milestone work, Hullin et al. [HHA*10] provided an adequate mathematical definition of the BBRRDF, which includes the reflection and the emission of light by a photoluminescence surface. Some research efforts have focused on finding a physically plausible analytical model for diffuse BBRRDFs. The diffuse model presented by Jung et al. [JHMD18] is simple, general and has successfully been applied to spectral upsampling [JWH*19]. Wilkie et al. [WWLP06] use a microfacet model to fit the diffuse behavior of a fluorescent surface observed during their experiment, which limits its general application. In contrast, in this work we first strive to create an analytical model for the behavior of a fluorescent nanoparticle applied to fluorescent volumetric scattering and to specular scattering by a rough surface modeled by a distribution of microfacets. Other works have strived to model fluorescent and phosphorescence effects for specific materials like ocean water or concentrators [Gla95, CS04, BHD*08, NSR17].

Fluorescent renderer. This second category of work is orthogonal to the previous one. The goal is the derivation of a rendering framework that can handle fluorescent scattering events. Indeed, fluorescence materials can lead to a wavelength shift in the light path, thus precautions need to be taken to simulate the light transport properly. Wilkie et al. [WTP01] have created a framework that can handle both fluorescence and polarization. Several improvements have been made since. Volumetric scattering with proper distance sampling for fluorescence events [MFW18] has been studied and bidirectional integrators have been defined [JA18, JHD20, GSMA08].

QD semiconductor nanoparticles. QD is a technology which attracts attention for its many applications. It has many advantages compared to fluorescent dyes. QDs have a high absorption in the non-visible UV wavelength range. In addition, QDs exhibit both a narrow emission spectrum, making its detection easier, and a high Quantum Yield. As such, they have been studied from both a chemistry and physics standpoint, and have found applications in many photonics technologies. In chemistry, the absorption and emission spectra of various QDs have been measured and empirical models describing their behavior as a function of their size or their molecular composition have been derived [LWMB02, BCNES05, YGC*19, GdlG09]. In physics, many works have investigated QD to understand and derive the fundamental interactions which explain their specific behavior. In pioneer works, Brus [Bru84, Bru86] has derived the physical equations which govern QD physics. Other works [Ken18, Ste57, VRS54] have also greatly contributed to the physical study of fluorescence.

We will present some of the results obtained by physics research in Section 3 as they constitute the foundation layer of our work.

Thin film coated surfaces. Rendering thin film coated surfaces has been the focus of several works [HKYM01, BP20, Sun06, SW08]. They use different methods or different approximations in either the number of internal reflections or the number of layers. The case of one layer thin film has been studied by Belcour and Barla [BB17] to render iridescence. Their model provides a fast and reliable way to perform spectral integration, enabling RGB iridescence rendering while avoiding spectral aliasing. Dhillon [Dhi21] also renders iridescence for periodic nanostructures obtained from scanned measurement. All those works try to account for the wave effects of light when interacting with a thin film. It is not the scope of our work. Instead, and this is a novelty of our approach, we are focusing on the energy transfers between the incident light, the nanoparticle and the underlying surface. To model these interactions, we resort to a thin film but we discard the interference wave effects to only account for energy coefficients. Our approach is closer to some other lines of work trying to model the influence of non-fluorescent nanoparticle coating on a surface. Vynck et al. [VPA*22] model the behavior of silicon nanoparticles on a surface. They derive a framework to account for the diffuse behavior of the particles, extending the work of Garcia et al. [GVGRB12] which simulated a similar situation without accounting for the diffuse scattering. Obviously, the configuration of their model is very different from ours as the size of their particle is much greater than ours and does not possess any fluorescent properties. As our particles are extremely small, we can discard the diffuse component of their scattering [GVHPTS13], only focusing on the specular component. Another work [SDHG16] derived their own BRDF for surfaces coated with small nanoparticles, with the constraints of ensuring exact energy equilibrium and reversibility of light propagation. In contrast, our work focuses on accounting for fluorescence which is an asymmetric event since a wavelength shift occurs along the lightpath, thus necessitating different precautions to ensure energy conservation. Also, we are not aiming to define a full new BRDF, but to derive a new Fresnel coefficient for a QD layered microfacet BRDF model to transform it into a BBRRDF, making our approach adaptable to various BRDF formulations.

Notation	Parameter	Value
E_{Gap}	Gap Energy (J)	$2.8e^{-19}$
E_{Coulomb}	Coulomb Energy (J)	/
$E_{\text{Confinement}}$	Confinement Energy (J)	/
e	Elementary charge (C)	$1.6e^{-19}$
h	Plank constant ($J.s$)	$6.63e^{-34}$
c	Light speed ($m.s^{-1}$)	$3.0e^{8}$
k_{B}	Boltzmann constant ($J.K^{-1}$)	$1.38e^{-23}$
m_e	Electon mass (kg)	$1.18e^{-31}$
m_h	Hole mass (kg)	$4.09e^{-31}$
ε_0	Vacuum permittivity ($F.m^{-1}$)	$8.85e^{-12}$
ε_r	Relative permittivity	5.8
$\mathcal{T}$	Temperature (K)	293
$\mathcal{R}$	QD Radius (nm)	$[1,5]$
λ	Wavelength (nm)	$[300,800]$
δ_λ	Standard deviation (nm)	15
S_λ	Stokes Shift (nm)	/
λ_{QD}	Threshold wavelength (nm)	/
$\mathcal{A}(\lambda)$	Absorption spectra	/
$\mathcal{E}(\lambda)$	Emission spectra	/
R	Energy Reflection Coefficient	$[0,1]$
$\mathcal{G}$	Gaussian function	/
$\mathcal{L}$	Logistic function	/
Λ	Logistic function primitive	/
V	QD volume (m^3)	/
m_{QD}	QD's refractive index	/
n_{QD}	Real part of m_{QD}	/
k_{QD}	Imaginary part of m_{QD}	/
f	Local field factor	/
$\sigma_{\text{sca}}^{\text{Ray}}$	Rayleigh scattering cross section	/
$\sigma_{\text{abs}}^{\text{Ray}}$	Rayleigh absorption cross section	/
σ_{abs}	Total absorption cross section	/
σ_{em}	Total emission cross section	/
Q	Quantum Yield	$[0,1]$
ρ	Coating density of QD	$[0,1]$

Table 1: *Variables and notations used throughout this work. The values are given for a CdSe QD*

3. Background

We start by presenting the fundamental theory on QD resulting from previous research which forms the foundations of our model. Mainly, we present two fundamental quantities. First is the analytical expression of the QD threshold wavelength λ_{QD} representing the threshold after which the QD does not absorb light. The second, is the expression of the Stokes shift S_λ representing the wavelength shift from the threshold wavelength λ_{QD} to the peak of the emission spectrum. All used notations are listed in Table 1. Example values are provided for Cadmium Selenide (CdSe) Quantum Dots as it is one of the most studied types of QDs.

3.1. Hypotheses

Our work uses several hypotheses. First, we only consider the Stokes shift and leave out the rare Anti-Stokes shift event. Therefore, the peak of the emission spectrum is always at a longer wavelength than that of the absorption spectrum. Second, we regard the wavelength dependent permittivity of the QD's to be independent of the QD size. We also assume that the QDs are in the strong confinement regime meaning that their size is smaller than the Bohr radius. The QDs are assumed spherical and all perfectly identical, thus omitting inhomogeneous broadening considerations. We will call upon those hypotheses in due time and introduce some others along with the related notions.

3.2. Threshold wavelength

To derive the mathematical expression of the threshold wavelength of the absorption spectrum, we need to describe the minimum possible energy of an absorbed photon $E_{\text{Absorption}}$. QDs are semiconductor nanocrystals. Like traditional bulk semiconductors, they

possess a conduction band and a valence band, the latter being filled with electrons. Those bands are separated by an energy gap E_{Gap} which depends on the QDs atomic composition. If a photon with an energy higher than the energy gap arrives on the semiconductors, it can be absorbed. An electron of the valence band will then be excited and promoted to the conduction band leaving a hole in the valence band. The electron-hole pair, possessing a negative and positive elemental charge respectively, is called an exciton. Because they possess electronic charges, the interaction between the particles of the exciton can be expressed with Coulomb potential energy denoted E_{Coul}. QDs have some special properties compared to the classic bulk semiconductors. The diameter of a QD is extremely small, only a few nanometers. The exciton is thus confined to a very small space. According to quantum mechanics theory, this configuration can be described as a particle in an infinite potential well. The solution to the Schrödinger equation under such conditions tells us that the confinement of the exciton within the nanocrystal results in some additional energy denoted E_{Conf}.

Thus the resulting minimum energy of the photon to interact with the QD is given by:

$$E_{\text{Absorption}} = E_{\text{Gap}} + E_{\text{Coul}} + E_{\text{Conf}} \tag{1}$$

$$with$$

$$E_{\text{Coul}} = \frac{-1.8e^2}{4\pi\varepsilon_0\varepsilon_r\mathcal{R}} \quad \text{and} \quad E_{\text{Conf}} = \frac{h^2(m_e+m_h)}{8\mathcal{R}^2 m_e m_h} \tag{2}$$

Equation 2 is called the Brus equation [SZS*19]. From here we can deduce the threshold wavelength of the QD using de Broglie relationship:

$$\lambda_{\text{QD}} = \frac{hc}{E_{\text{Absorption}}} \tag{3}$$

We have now obtained the maximum threshold wavelength λ_{QD} for the absorption of the QD. We can observe that λ_{QD} varies with the radius $\mathcal{R}$ of the QD, in other words the larger the Quantum Dot, the longer is the threshold wavelength. Having defined λ_{QD}, we can now derive the expression for the Stokes shift.

3.3. Absorption and Emission Spectra

The absorption spectrum of the QD can be divided into two components. The first part is the bulk absorption that results from the molecular composition of the QD. This absorption spectrum, which is derived in the next section, has a cut-off wavelength of λ_{QD} due to the quantum confinement. The second part of the absorption occurs around the threshold wavelength. It is called the quantum absorption and is denoted as $\mathcal{A}_{\text{QD}}(\lambda)$. As shown in previous work [TIS*20, TGSR22], the quantum absorption can be modeled by a Gaussian function centered on λ_{QD}. The standard deviation of the Gaussian depends on the homogeneous broadening of the Quantum Dot but is usually very small - around 15 nm - creating a narrow absorption peak around λ_{QD}. The QD emission spectrum denoted $\mathcal{E}_{\text{QD}}(\lambda)$ can also be modeled by a Gaussian function with a center around $\lambda_{\text{QD}} + S_\lambda$, where S_λ is the Stokes shift. So we can express the quantum absorption and emission spectrum as follows:

$$\mathcal{A}_{\text{QD}}(\lambda) \propto \exp\left(-\frac{(\lambda-\lambda_{\text{QD}})^2}{\delta_\lambda^2}\right) \tag{4}$$

$$\mathcal{E}_{\text{QD}}(\lambda) \propto \exp\left(-\frac{(\lambda-\lambda_{\text{QD}}-S_\lambda)^2}{\delta_\lambda^2}\right) \tag{5}$$

Leveraging the Kennard–Stepanov relationship [Ken18] which provides an analytical expression for the ratio of the quantum absorption spectrum over the emission spectrum, the Stokes shift can be expressed as [TR15]:

$$S_\lambda = \frac{hc}{k_{\text{B}}T}\frac{\delta_\lambda^2}{\lambda_{\text{QD}}^2} \tag{6}$$

At this point, we would like to highlight some immediate outcomes. First, we can see that two parameters control the wavelength around which the emission spectrum is centered: the radius $\mathcal{R}$ of the QD and the standard deviation δ_λ of the absorption and emission Gaussian distributions. While the standard deviation of the emission spectrum is normally a fixed physical property, it can easily be modified as an artist parameter in a rendering context. Second, modeling the emission and absorption spectra as Gaussian distributions is a common approach in Optics literature consistent with the physical measurements [TIS*20].

Using this background and these expressions we now proceed to derive a model for the bulk absorption in order to fully represent the absorption spectrum.

4. Our model

We describe fluorescence using an absorption and an emission spectrum. It can easily be converted to a re-radiation matrix if need be. We articulate our model in two components. The first is the application of our QD framework to fluorescent volumetric scattering. The second part is dedicated to the derivation of our fluorescent specular microfacet reflection model.

4.1. Volumetric Absorption and Emission

A QD is a semiconductor nanoparticle of radius ranging from 1 to 5 nanometers, thus they are very small compared to the visible light wavelength ($380-780$ nm). As such, they fall within Rayleigh's approximation for small particle absorption and scattering, whose scattering and absorption cross sections are given by [LWMB02]:

$$\sigma_{\text{sca}}^{\text{Ray}}(\lambda_i) = \frac{24\pi^3V^2}{\lambda_i^4}\left|\frac{m_{\text{QD}}^2-m_{\text{env}}^2}{m_{\text{QD}}^2+2m_{\text{env}}^2}\right| \quad \sigma_{\text{abs}}^{\text{Ray}}(\lambda_i) = \frac{4\pi n_{\text{env}}k_{\text{QD}}|f|^2V}{\lambda_i} \tag{7}$$

where V is the volume of a QD given by $\frac{4}{3}\pi\mathcal{R}^3$, k_{QD} is the imaginary part of the QD's complex refraction index noted m_{QD}, and n_{env} is the real part of the environment complex index of refraction m_{env}. k_{QD}, n_{env}, m_{QD} and m_{env} are functions of the incoming wavelength λ_i. f is the local field factor given by:

$$f = \frac{3m_{\text{env}}^2}{m_{\text{QD}}^2 + 2m_{\text{env}}^2} \tag{8}$$

Because of the small radius of the QD compared to the wavelength of interest, the $\frac{V^2}{\lambda^4}$ factor in the scattering cross section expression makes it very small compared to the absorption cross section. Thus we can neglect scattering from any further consideration.

As mentioned earlier, the absorption spectrum of a QD has a Gaussian distribution, that we denote $\mathcal{G}$, around the cut-off wavelength. We model the total absorption cross section σ_{abs} by combining Rayleigh's absorption with the quantum absorption defined in Section 3.3 in the following manner:

$$\sigma_{\text{abs}}(\lambda_i) = \begin{cases} \sigma_{\text{abs}}^{\text{Ray}}(\lambda_i) + \frac{1}{2}\beta\mathcal{G}(\lambda_i, \lambda_{\text{QD}}, \delta_\lambda) & \text{if } \lambda_i \leq \lambda_{\text{QD}} \\ \frac{3}{2}\beta\mathcal{G}(\lambda_i, \lambda_{\text{QD}}, \delta_\lambda) & \text{otherwise} \end{cases} \tag{9}$$

$$\text{with} \quad \beta = \sigma_{\text{abs}}^{\text{Ray}}(\lambda_{\text{QD}})$$

The β coefficient ensures the continuity of the spectrum at λ_{QD}. Plots of the absorption spectra are shown in Section 5.1. Now that we have established an expression for the absorption cross section, we next derive one for the emission cross section due to the photoluminescence of the QD. As a first step, we approximate the Gaussian shape of the emission spectrum by a logistic distribution [CBTB15]. The latter has two benefits, the logistic function is easy to sample and is analytically integrable. The integral of the logistic function is denoted Λ and its expression is detailed in Appendix A. The emission cross-section is:

$$\sigma_{\text{em}}(\lambda_o) = \gamma\mathcal{L}(\lambda_o, \lambda_{\text{QD}} + S_\lambda, \frac{\delta_\lambda}{2}) \tag{10}$$

Where γ is a scaling coefficient ensuring conservation of energy.

Energy is conserved if the total emitted energy over the spectrum is lower than the total absorbed energy over the spectrum. We can ensure that the probability of a photon being re-emitted due to fluorescence over the mean free path is less than the probability of a photon being absorbed over the same distance. In other words, the integral of the emission cross section over the spectrum needs to be less than the integral of the total absorption cross section over the spectrum.

$$\int_{\lambda_{\min}}^{\lambda_{\max}} \sigma_{\text{em}}(\lambda_o)\, d\lambda_o \leq \int_{\lambda_{\min}}^{\lambda_{\max}} \sigma_{\text{abs}}(\lambda_i)\, d\lambda_i \tag{11}$$

We can write the integral of the emission cross section over the spectrum as:

$$\int_{\lambda_{\min}}^{\lambda_{\max}} \sigma_{\text{em}}(\lambda_o)\, d\lambda_o = \gamma I \tag{12}$$

$$with$$

$$I = \Lambda(\lambda_{\max}, \lambda_{\text{QD}} + S_\lambda, \frac{\delta_\lambda}{2}) - \Lambda(\lambda_{\min}, \lambda_{\text{QD}} + S_\lambda, \frac{\delta_\lambda}{2}) \tag{13}$$

Then the inequality in Equation 12 becomes:

$$\gamma I \leq \int_{\lambda_{\min}}^{\lambda_{\max}} \sigma_{\text{abs}}(\lambda_i)\, d\lambda_i \tag{14}$$

To find the final value of γ, we use a physical parameter called the Quantum Yield (QY) denoted Q. This parameter ranges from 0 to 1 and represents the effectiveness of the conversion of an absorbed photon into a re-emitted photon. A QD generally exhibits QY values around 80% which is very high among fluorescent materials. We can now write a final expression for γ:

$$\gamma = \frac{Q}{I} \int_{\lambda_{\min}}^{\lambda_{\max}} \sigma_{\text{abs}}(\lambda_i)\, d\lambda_i \tag{15}$$

We have now derived the absorption and emission coefficients for fluorescent volumetric rendering. They compose the first part of our framework. Renderings are presented in Section 6.2. In the following section we present the second part of our model, which is a specular microfacet fluorescence BBRRDF model.

4.2. Microfacet BBRRDF

In the following section we define a new BBRRDF model for specular fluorescence microfacet reflection. To do so, we calculate a new Fresnel coefficient that makes our approach adaptable to various BRDF formulations, and allows us to extend their formulation to support fluorescence. In a stepwise fashion, we start by introducing the configuration for our model in Section 4.2.1. Then we define the optical properties of the thin film representing the QD coating (Section 4.2.2). Finally, in Section 4.2.3, we derive a new Fresnel coefficient by studying how the thin film affects the reflection properties of the underlying material.

4.2.1. Model Configuration

Let us consider a non-magnetic rough surface with a complex refractive index m_{sub} which can be described by a distribution of microfacets. We will refer to this surface as substrate. Let us add on top of this substrate a monolayer of perfectly identical spherical QD nanoparticles, randomly distributed with a density ρ varying from 0 to 1. If the density is 0, there is no QD on the surface, if $\rho = 1$, the surface is entirely coated with QDs. We investigate how the QD's coating of the microfacet surface modifies the Fresnel coefficients of the substrate. The situation is illustrated in Figure 2.

It is important to note here that we are only interested in the specular response of the QD nanoparticles and we will not consider the diffuse behavior. This assumption is valid because the QDs are very small compared to the incident light wavelength. Indeed, in this case, the energy of the diffuse reflection is much lower than

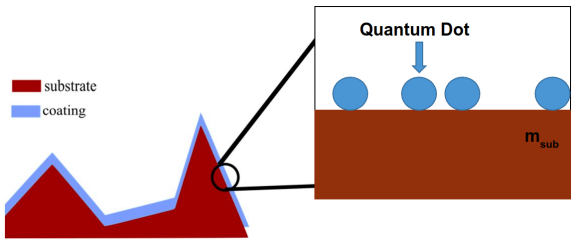

Figure 2: *Illustration of the nanometer scale fluorescent material. QDs are nanoparticles considered identical and spherical. They are coated on the substrate as a monolayer with variable density. The geometry of the surface can be described by a microfacet BRDF.*

the specular reflection energy [GVHPTS13]. As for the re-emitted energy, it has been shown that QD coated surfaces can be carefully designed to mainly reemit in the specular reflection direction - about 85% - and a little in the retro-reflection direction [CVT*10]. We will only model the main reflected contribution. As such, within the microfacet reflection model, we can consider that the addition of the QDs only modifies the energy of the reflected light, not its direction. Thus, we solely contemplate the Fresnel term of the microfacet model.

To calculate the new Fresnel coefficients of the coated substrate, we assimilate the discrete coating of QD nanoparticles to a continuous thin film [SDHG16, GVHPTS13]. This thin film of thickness equal to the diameter of the QDs is placed above the substrate, the two being separated by an infinitely thin layer of the environment medium. This configuration illustrated in Figure 3 will be used to model the multiscattering events between the substrate and the QD nanoparticles. The physical properties of the thin film will be described as a function of the density of nanoparticles ρ.

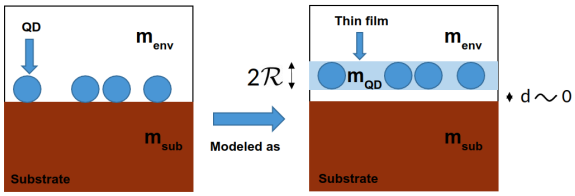

Figure 3: *Illustration of our modeling of the QD-coated fluorescent material. Left is the representation of the physical situation. Right is our model of the material where the continuous thin film serves as a representation of the discrete QD coating.*

4.2.2. Thin film Reflection and Transmission

To derive the energy reflection and transmission coefficients of the thin film, we consider the monolayer of QDs placed in the environment medium without any substrate. In which case, the coefficients for the s and p polarized reflection can be expressed as [WBST99]:

$$r^s_{\text{spe}}(\theta,\lambda) = \frac{-\alpha(\theta,\lambda)S_s(\theta,\lambda)}{1+\alpha(\theta,\lambda)} \quad r^p_{\text{spe}}(\theta,\lambda) = \frac{-\alpha(\theta,\lambda)S_p(\theta,\lambda)}{1+\alpha(\theta,\lambda)} \tag{16}$$

$$\alpha(\theta,\lambda) = \frac{\rho\lambda^2}{2\pi^2\mathcal{R}^2 n^2_{\text{env}}\cos(\theta)} \tag{17}$$

Where ρ is the density of QDs, θ the incident angle, $\mathcal{R}$ the radius of the QDs. S_s, S_p and S_0 are the amplitude scattering coefficients for a single particle which can be expressed as [BH08]:

$$S_s = S_0 = -i\left(\frac{2\pi\mathcal{R}n_{\text{env}}}{\lambda}\right)^3 \frac{m^2_{\text{QD}} - m^2_{\text{env}}}{m^2_{\text{QD}} + 2m^2_{\text{env}}} \quad S_p = S_0\cos(\pi - 2\theta) \tag{18}$$

Now we have the amplitude of the specular reflection coefficients of our thin film. To obtain the energy coefficients for unpolarized light, we use the usual formulas:

$$R_{\text{spe}} = \frac{1}{2}(||r^s_{\text{spe}}||^2 + ||r^p_{\text{spe}}||^2) \quad \text{and} \quad T_{\text{spe}} = 1 - R_{\text{spe}} \tag{19}$$

With an approach similar to the one used to obtain Equation 9, we start by deriving the bulk absorption of the thin film during a single propagation of the light through the thin film. To do so, we use the Beer-Lambert law of attenuation which gives us:

$$\mathcal{A}^{\text{bulk}}_{\text{tf}}(\lambda_i) = \exp\left(\frac{-4\pi k_{\text{QD}} l}{\lambda_i}\right) \quad \text{with} \quad l = \frac{2\mathcal{R}\rho}{\cos(\theta_t)} \tag{20}$$

Where l represents the average distance traveled by the light through the thin film and is proportional to the density of the coating ρ. θ_t is the refracted light angle. We can now express the absorption spectrum of the QD thin film following the same principle as in Section 4.1.

$$\mathcal{A}_{\text{tf}}(\lambda_i) = \begin{cases} \exp\left(\frac{-4\pi k_{\text{QD}} l}{\lambda_i}\right) + \beta\mathcal{G}(\lambda_i, \lambda_{\text{QD}}, \delta_\lambda) & \text{if } \lambda_i \leq \lambda_{\text{QD}} \\ 2\beta\mathcal{G}(\lambda_i, \lambda_{\text{QD}}, \delta_\lambda) & \text{otherwise} \end{cases} \tag{21}$$

$$\beta = \exp\left(\frac{-4\pi k_{\text{QD}} l}{\lambda_{\text{QD}}}\right)$$

With β representing a coefficient that ensures continuity of the curve at λ_{QD}.

We have established the reflection, transmission and absorption energy coefficients of the thin film. The thin film is placed on top of the substrate assuming a sub-nanometer interstitial layer of environment medium between the two. This interstice is considered small enough to neglect absorption and to assume that the multiscattering events remain localized at the point of intersection. The

situation is illustrated in Figure 4. We calculate the total reflection and absorption energy coefficients resulting from the multiscattering events occurring between the thin film and the substrate.

4.2.3. Total Reflected and Absorbed Energy

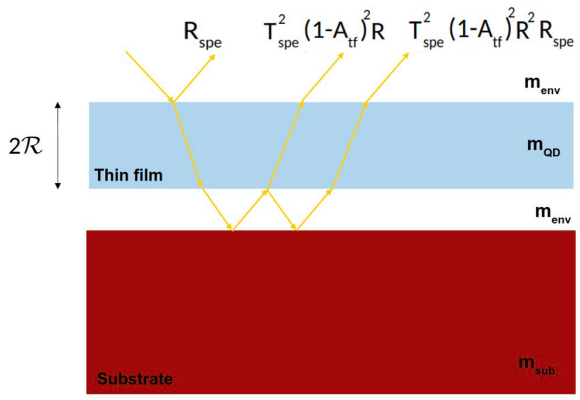

Figure 4: *Representation of the multiscattering events that occur between the thin film and the substrate.*

To derive the total reflected and absorbed energy from the multiple scattering between the substrate and the thin film, we will use an energy approach. This means that we will discard the phase delay introduced by the thin film, thus removing any interference effect. In practice, this assumption is correct as the thin film is very thin compared to the light wavelength, thus only introducing a very small delay. Another important point is that the reflection, transmission and absorption energy coefficients of the thin film derived earlier apply to the entire thin film, not to the thin film-environment interface. Also, though not shown in the following equations for the sake of notation clarity, energy coefficients depend on the wavelength and on the incident angle. Using the same notations as in the previous section and denoting R to be the reflection coefficient between the substrate and the environment medium we can calculate that the multiple scattering between the thin film and the substrate yields:

$$\begin{aligned} R_{\text{tot}} = R_{\text{spe}} + T_{\text{spe}}^2(1-\mathcal{A}_{\text{tf}})^2 R + T_{\text{spe}}^2(1-\mathcal{A}_{\text{tf}})^2 R^2 R_{\text{spe}} \\ + T_{\text{spe}}^2(1-\mathcal{A}_{\text{tf}})^2 R^3 R_{\text{spe}}^2 + \dots \end{aligned} \tag{22}$$

Which gives us

$$R_{\text{tot}} = R_{\text{spe}} + \frac{T_{\text{spe}}^2(1-\mathcal{A}_{\text{tf}})^2 R}{1 - R R_{\text{spe}}} \tag{23}$$

Similarly we can calculate the total absorbed energy of the thin film which gives us:

$$\mathcal{A}_{\text{tot}} = T_{\text{spe}}\mathcal{A}_{\text{tf}} + \frac{T_{\text{spe}}\mathcal{A}_{\text{tf}} R T_{\text{spe}}(1-\mathcal{A}_{\text{tf}})}{1 - R R_{\text{spe}}} \tag{24}$$

Now that we have calculated the total absorbed energy, we can derive an expression for the emission spectrum. Proceeding in a similar manner as in Section 4.1 to ensure energy conservation, we obtain:

$$\mathcal{E}_{\text{tot}}(\theta, \lambda_o) = \gamma(\theta)\mathcal{L}(\lambda_o, \lambda_{\text{QD}} - S_\lambda, \frac{\delta_\lambda}{2}) \tag{25}$$

with

$$\gamma(\theta) = \frac{Q}{I}\int_{\lambda_{\text{min}}}^{\lambda_{\text{max}}} \mathcal{A}_{\text{tot}}(\theta, \lambda_i)\, d\lambda_i \tag{26}$$

We now have all the elements to define our new bispectral Fresnel coefficient $F(\theta, \lambda_i, \lambda_o)$ which we express as:

$$F(\theta, \lambda_i, \lambda_o) = R_{\text{tot}}(\theta, \lambda_i) + \mathcal{A}_{\text{tot}}(\theta, \lambda_i)\mathcal{E}_{\text{tot}}(\theta, \lambda_o) \tag{27}$$

Using this Fresnel function we define a new microfacet BBRRDF model in the following way:

$$BBRRDF(\omega_i, \omega_o, \lambda_i, \lambda_o) = \frac{D(\omega_h)G(\omega_i, \omega_o)F(\omega_i, \lambda_i, \lambda_o)}{4 < \omega_i, n >< \omega_o, n >} \tag{28}$$

With this we have fully derived our specular fluorescent microfacet surfaces reflection model. Next, we demonstrate the influence of the parameters of the model as well as its validity.

5. Validations

The validity of our model is investigated from three angles. In Section 5.1, we present the absorption and emission cross-section spectra obtained for volumetric rendering and show that the evolution of those spectra with respect to the radius of the QDs and the width of the emission spectrum behave as expected. We qualitatively compare our model to measurements obtained in physical experiments and show that they exhibit close resemblance (see Appendix B). In Section 5.2, we conduct the same study for the QD coating. We demonstrate how the coating affects the reflection properties of the underlying substrate. Finally, Section 5.3 focuses on fitting our fluorescent microfacet model to the BRDF measurement obtained by Dupuy and Jakob [DJ18] for white paper. In their measurement, they assumed a microfacet description of the underlying material and then performed a measurement of the BRDF. Because white paper possesses fluorescent properties, their measurement of the material leads to results that, if used directly in rendering, breaks energy conservation. We show that using our model, we are able to fit the measurement obtained by Dupuy and Jakob [DJ18] and thus use it in rendering without creating excessive energy.

5.1. Volume Cross Section

We present the influence of the radius $\mathcal{R}$ of the Quantum Dot and the standard deviation of the emission spectra δ_λ on the absorption and emission cross section spectrum in Figure 5 and Figure 6.

Our model generated the spectra illustrated Figure 5. They show

that as the size of the QD increases, the value of λ_{QD} and the emission spectrum shifts toward the longer wavelength which matches the actual QD behavior. The observed superposed portions in the absorption spectra is a consequence of the assumption made in our model that the permittivity of a QD is independent of its size. We see that our model conserves the main elements of the QD behavior: (i) High absorption in UV; (ii) A cut-off wavelength which increases with the radius of the QD; (iii) A Gaussian profile around the cut-off wavelength; (iv) A Gaussian emission spectrum centered on a wavelength which increases with the radius $\mathcal{R}$ of the QD.

We qualitatively compare the absorption and emission spectrum obtained here to measured ones in [GBS*16, CVR*19, SN04] in Figure 18, Figure 19 and Figure 20 respectively.

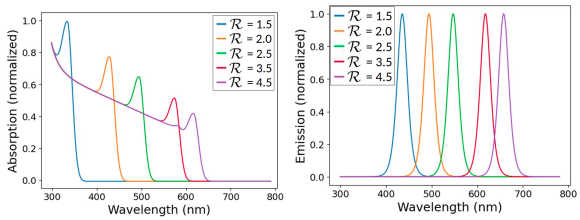

Figure 5: *Effect of the QD radius $\mathcal{R}$ on the absorption and emission cross section spectra. Normalized absorption (left) and emission (right) cross section spectra for $\mathcal{R}$ varying from 1.5 nm (blue) to 4.5 nm (purple) with a constant $\delta_\lambda = 15nm$.*

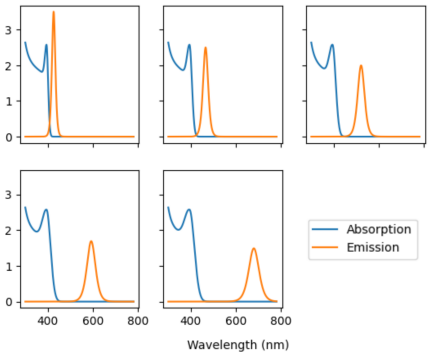

Figure 6: *Effect of manipulating the standard deviation of the emission spectrum δ_λ on the absorption and emission cross section spectra. Evolution of the absorption and emission cross section spectra for different $\delta_\lambda = \{10, 15, 20, 25, 30\}$ nm with a constant QD radius $\mathcal{R} = 1.8$ nm.*

Figure 6 shows that as the emission standard deviation increases, the Stokes shift increases as well. The maximum of the emission spectrum decreases as anticipated to insure energy conservation.

5.2. Fluorescent Specular Microfacet

We illustrate how the QD coating modifies the Reflection coefficient of the underlying substrate. The evolution of the absorption and emission spectra with the radius $\mathcal{R}$ of the QDs is the same as for the volume cross section presented in Figure 5. In Figure 7, we show the absorption and emission spectra as well as the re-radiation matrix which is obtained by multiplying the absorption with the emission for all input/output wavelength configurations.

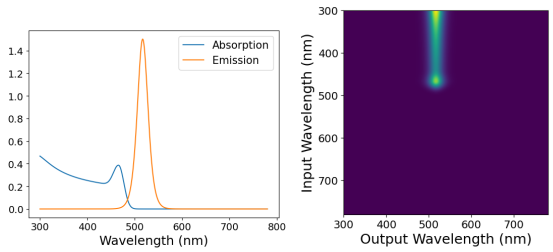

Figure 7: *Absorption and Emission spectra for the QD coating and re-radiation matrix representation obtained from those spectra. Left: Total absorption and emission spectra $\mathcal{A}_{tot}$ and $\mathcal{E}_{tot}$ of the thin film coating. QD parameters: $\mathcal{R} = 2.2$ nm, $\delta_\lambda = 15$ nm, $\rho = 0.5$, $Q = 0.8$. Right: Re-radiation matrix representation obtained by multiplying $\mathcal{A}_{tot}$ to $\mathcal{E}_{tot}$ for each input-output wavelengths.*

The QDs introduce absorption which we present in Figure 8. In this figure we show the absorption due to a single interaction with the thin film ($\mathcal{A}_{tf}$) and the one due to the multiple scattering between the substrate and the thin film ($\mathcal{A}_{tot}$).

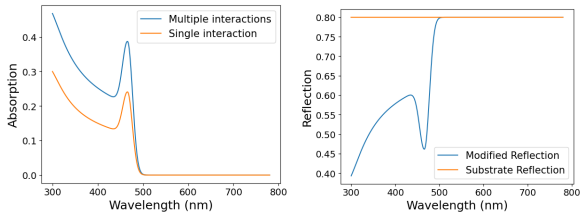

Figure 8: *Effect of QD coating on absorption and reflection. Left: Absorption spectra for a single interaction $\mathcal{A}_{tf}$ (orange) and multiple interactions $\mathcal{A}_{tot}$(blue) between the incident light and the thin film. Right: Material reflection without thin film coating R (orange) and with thin film coating R_{tot} (blue). QD parameters: $\mathcal{R} = 2.2$ nm, $\delta_\lambda = 15$ nm, $\rho = 0.5$, $Q = 0.8$.*

We also compare in Figure 8, R, the Fresnel reflection coefficient of the substrate with R_{tot}, the modified reflection including the effect of the thin film. Here R was set constant and all the differences between R and R_{tot} are due to the QD coating. We can see that the absorption introduced by the thin film causes a decrease in the reflection coefficient of the original substrate.

In Figure 9, we present the emission spectrum $\mathcal{E}_{tot}$ together with R_{tot}. This Figure is similar to the measured spectra shown by Rossier [Ros13]. In the next section, we fit this curve to the BRDF measurement of white paper presented by Dupuy and Jakob [DJ18].

5.3. Modeling White Paper

In this final step of the validation work, we want to show that our model can be used to represent real measurement of fluorescent ma-

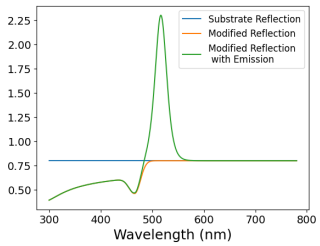

Figure 9: *Representation of the substrate reflection spectrum R (blue), the modified reflection spectrum R_{tot} (orange) and the modified reflection plus the emission spectrum $R_{tot} + \mathcal{E}_{tot}$ (green). QD parameters $\mathcal{R} = 2.2$ nm, $\delta_\lambda = 15$ nm, $\rho = 0.5$, $Q = 0.8$. The modified reflection with emission spectrum in green is very similar to what is obtained when measuring the reflection of fluorescent materials [Ros13].*

terials. In the database provided [DJ18], one of the measured materials is white paper which possesses strong fluorescent properties. Indeed, to appear whiter, standard non-fluorescent paper is coated with Optical Brightening Agents. Those agents are fluorescent dyes which absorb UV light and re-emits in the blue range of the visible spectrum. Although those dye molecules are not precisely QD nanocrystals, our model, approximating QDs to a thin film, can still represent their behavior. Since the measurements assume a microfacet representation of the measured surface, our model is a perfect fit to properly render white paper while properly accounting for the fluorescence. In this section, we illustrate the fitting of the measurements in Figure 10. Rendering results are demonstrated in the next section.

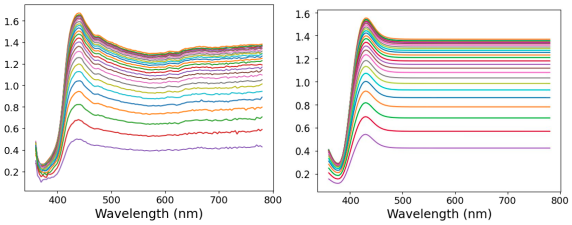

Figure 10: *Fitting our specular fluorescent reflection coefficient to white fluorescent paper reflection measurements. We fit our model (right) to the measured reflection of fluorescent white paper (left) for different reflection directions (the incident light direction is constant). To obtain a better fit, we had to enlarge the emission spectrum as the QDs have a very narrow spectrum compared to other fluorescent materials. We thus multiply δ_λ by 2 in Equation 4 and 5.*

In their work, Dupuy and Jakob. provide reflection measurements for multiple incident and reflection angles. To reproduce them with our model, we try to find the values of Q, δ_λ, $\mathcal{R}$ and ρ that provide the best fit. Since paper can not be described by an index of refraction, we set the value of R to the average value of the reflection measurement over the range 650 to 780 nanometers where there is no re-emission. We found that $Q = 0.22$, $\delta_\lambda = 12$ nm and $\mathcal{R} = 1.68$ nm fit the measurements well.

6. Results

We present here our rendering results. We illustrate both the volumetric rendering and the specular fluorescent rendering. We will show the influence of different parameters on the final appearance, like the roughness of the microfacet distribution, the density of QD coating, the Quantum Yield and the QD radius. But we first start by describing our implementation.

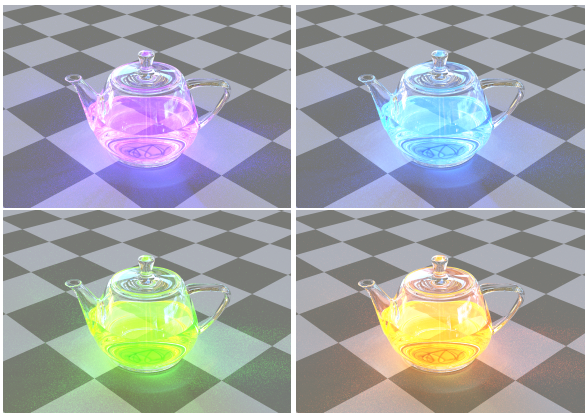

Figure 11: *Fluorescent volume rendering of solutions of CdSe QD in chloroform illuminated with a UV light with constant intensity over the 300nm to 380 nm range and an environment visible light. QDs of varying radii are shown. Top left: $\mathcal{R} = 1.5$ nm, top right $\mathcal{R} = 1.75$ nm, bottom left $\mathcal{R} = 2.7$ nm, bottom right $\mathcal{R} = 3$ nm. The other parameters are constant and set to: $Q = 0.8$, $\delta_\lambda = 15$ nm and an isotropic phase function is used. The concentrations are scaled to obtain similar fluorescent intensity for all solutions.*

6.1. Implementation

Our model is implemented using the ART renderer [ART18] and Mitsuba renderer [Jak10]. For sampling the wavelength shift, we sample the emission spectrum analytically and the absorption spectrum numerically. We considered the probability of shifting wavelength to be equal to the value of the absorption spectrum. The absorption spectrum is precomputed for each incident angle and each wavelength. We also specify as an input the integration range over which we integrate the absorption spectrum to normalize the emission spectrum to ensure energy conservation i.e. λ_{min} and λ_{max} in Equations 11 and 26.

6.2. Fluorescent Volume Rendering

We start by illustrating the fluorescent volume rendering capabilities of our model in Figure 11 and Figure 12. We render CdSe based QDs dispersed in a chloroform solution. The CdSe QDs can be excited over a broad range of wavelengths and emit with a narrow peak, yielding emission that spans over the entire visible spectrum. Here we render CdSe QDs of different radii under two illumination settings. Figure 11 shows CdSe QDs solutions illuminated by a constant UV light (300 to 380 nm) and an environment map covering the entire visible spectrum while Figure 12 shows the same setting without the environment map. We observe that the color of

the solution shifts towards a longer wavelength as the radius increases, confirming again the size-dependent spectral properties of the QDs.

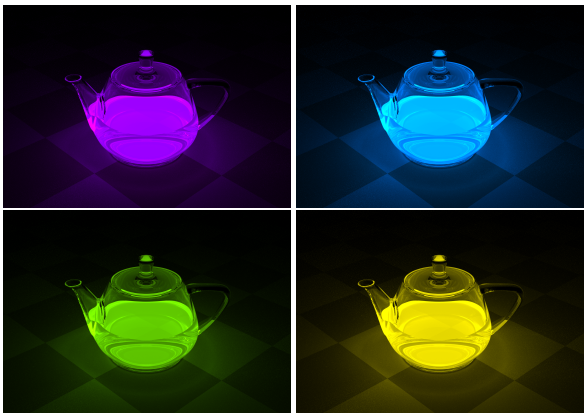

Figure 12: *Same solutions as in Figure 11 but illuminated only with a constant UV light. The color results from the emission of the QDs only.*

6.3. Specular Fluorescent Microfacet Rendering: Application to White Paper

We now demonstrate the specular fluorescent microfacet BBRRDF results. In addition to the validation data presented in Section 5.3, we illustrate how our model can be used to simulate the appearance of white paper. Paper is a complex material to represent [Far09]. Here, we model it as a rough dielectric surface using a microfacet BRDF. Presented in Figure 13 are the renderings of two sheets of paper, one with a constant reflection coefficient over the visible spectrum (on the left) and another using the same description but adding a QD coating using our model. We render the scene using two different lighting conditions, a constant light over the visible spectrum and a constant UV light. We can see that the paper coated with the QDs appears whiter than the uncoated one. Simulating the actual paper coated with Optical Brightening Agents, the paper absorbs the UV light and emits at low visible wavelengths as rendered in Figure 13.

6.4. Specular Fluorescent Microfacet BBRRDF Rendering

We illustrate here how the different built-in parameters allow a refined control over the final appearance. Figure 14 illustrates the effect of modifying the radius $\mathcal{R}$ of the QDs and the standard deviation δ_λ. As detailed in previous sections, both parameters control the Stokes shift value, thus the central wavelength of the emission spectrum and consequently, the rendered color. But modifying $\mathcal{R}$ modifies the center of the absorption while modifying δ_λ leaves it unchanged thus explaining the differences in appearances.

Figure 15 illustrates the effect of modifying the density ρ of the QD coatings for two materials having very different roughness and QD coatings. The ball placed the farthest on the left is the material without any coating ($\rho = 0$). As we move to the right, the density

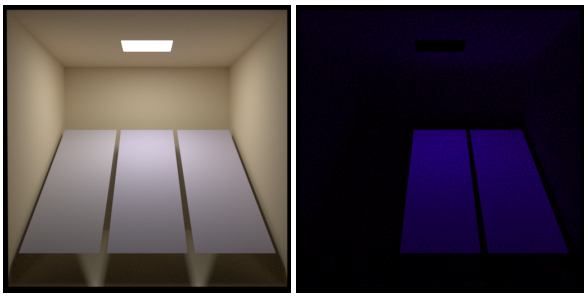

Figure 13: *Applying our specular fluorescent microfacet BBRRDF to white paper rendering. Each image above shows three white paper sheets rendered side by side. On the left, using a microfacet model without Brightening Agents. In the middle the same configuration with Brightening Agents modeled by QDs. On the right, using a diffuse representation [JHMD18] with Brightening Agents modeled using the same emission and absorption spectra and $Q = 1$ and $c = 1$. Scene is rendered under two illumination conditions. Left image: constant visible spectrum and UV light. Right image: constant UV light.*

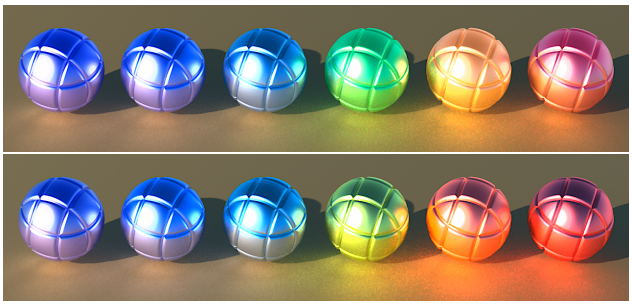

Figure 14: *Top: Our model with different QDs radii $\mathcal{R} = \{1.5, 1.75, 2, 2.7, 3.3, 5\}$ nm with $\delta_\lambda = 15$ nm $Q = 0.8$ $\rho = 0.5$. Bottom: Our model with different standard deviation $\delta_\lambda = \{15, 16.5, 18, 21, 24, 27\}$ nm with $\mathcal{R} = 1.5$ nm $Q = 0.8$ $\rho = 0.5$. Emission is scaled for all QDs to appear having the same brightness.*

of the coating increases, thus the absorbed and emitted energy also increases.

Figure 16 illustrates the effect of modifying the Quantum Yield Q of the QDs for two materials having very different roughness but the same QD coating. The ball placed the farthest on the left has a coating but the Quantum Yield is set to 0, so there is no emission, just absorption. As we move to the right, the Quantum Yield increases, thus the emitted energy increases.

Figure 17 illustrates the effect of modifying the roughness of the material for a constant QD coating. The ball placed the furthest on the left has a very low roughness and as we move to the right, the roughness increases.

7. Limitations and Future Work

We have demonstrated how our QD rendering model can be used to render fluorescent volumes and specular fluorescent microfacet

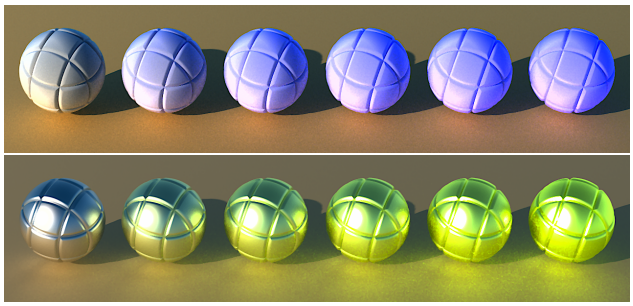

Figure 15: *Our model with different QD coatings density* ρ $\{0, 0.2, 0.4, 0.6, 0.8, 1\}$ *for two different surface roughness and QD coatings (top: high roughness with* $\mathcal{R} = 1.5$ *nm* $\delta_\lambda = 15$ *nm* $Q = 0.8$*) (bottom : low roughness with* $\mathcal{R} = 2.7$ *nm* $\delta_\lambda = 15$ *nm* $Q = 0.8$*).*

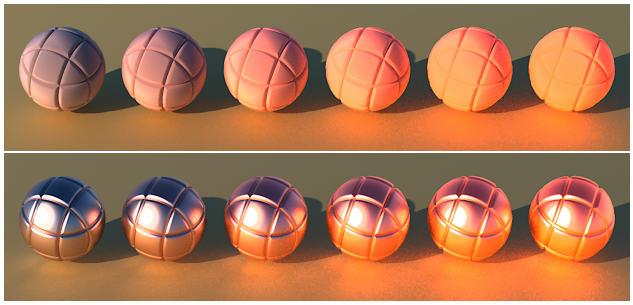

Figure 16: *Our model with different QD Quantum Yield* $Q = \{0, 0.2, 0.4, 0.6, 0.8, 1\}$ *for two different surface roughness but with the same QD coating (top: high roughness), (bottom : low roughness) with* $\mathcal{R} = 3.3$ *nm* $\delta_\lambda = 15$ *nm* $\rho = 0.5$*.*

modeled surfaces. One limit of our model is to consider the QD's permittivity independent of the radius. Removing this limitation would improve the accuracy of our model. Another limit of our model is to only consider the emission in the reflection direction and not the part that is retro reflected. This part accounts for around 15% of the re-emitted energy. We believe our work can be extended in multiple ways. A possible extension would be to develop a parametrization of our model that would be more suitable for artistic editing. Another research direction would be to perform spectral integration to render fluorescence in RGB along the lines of the work of Belcour and Barla [BB17] This would be a great step toward integrating fluorescence into real-time rendering. Another interesting direction of exploration would be to derive fluorescent coefficients for specular transparent fluorescent objects. Finally, another extension would be to alleviate the specular fluorescence assumption and consider a diffuse fluorescent emission based on a microfacet surface distribution. Although the majority of our derivation would remain valid, this would lead to defining a BBRRDF based on an Oren–Nayar model.

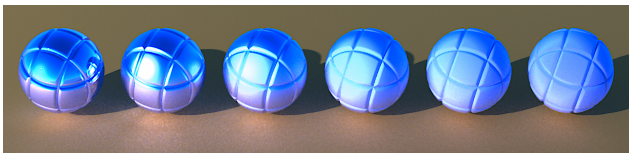

Figure 17: *Our model for surfaces of different roughness* $\{0.05, 0.1, 0.4, 0.6, 0.8, 1\}$ *with identical QD coatings* $\mathcal{R} = 1.75$ *nm* $\delta_\lambda = 15$ *nm* $\rho = 0.5$*,* $Q = 0.8$*.*

8. Conclusion

In this paper we have presented an analytical, physically based rendering framework for Quantum Dots (QDs) nanoparticles that allowed us to render fluorescent volumes and QD coated material surfaces. Our approach involves simulating the behavior of a surface coated with QDs to derive a new Bispectral Bidirectional Reflection and Reradiation Distribution Function (BBRRDF) for microfacet models. Our results show that our model can represent fluorescent materials and we have demonstrated its effectiveness in rendering both fluorescent volumes and specular fluorescent microfacet surfaces. Our model is versatile and allows for the adjustment of the physical parameters to achieve a wide range of fluorescent colors and appearances.

9. Acknowledgement

The authors would like to thank Activision Publishing and the engineering team of High Moon Studios for supporting this research project.

References

[ART18] The advanced rendering toolkit, 2018. https://cgg.mff.cuni.cz/ART/. 9

[BB17] BELCOUR L., BARLA P.: A practical extension to microfacet theory for the modeling of varying iridescence. *ACM Transactions on Graphics 36*, 4 (July 2017), 65. 3, 11

[BCNES05] BURDA C., CHEN X., NARAYANAN R., EL-SAYED M. A.: Chemistry and properties of nanocrystals of different shapes. *Chemical reviews 105*, 4 (2005), 1025–1102. 2

[BH08] BOHREN C. F., HUFFMAN D. R.: *Absorption And Scattering Of Light By Small Particles*. John Wiley & Sons, 2008. 6

[BHD*08] BENDIG M., HANIKA J., DAMMERTZ H., GOLDSCHMIDT J. C., PETERS M., WEBER M.: Simulation of fluorescent concentrators. In *2008 IEEE Symposium on Interactive Ray Tracing* (2008), pp. 93–98. 2

[BP20] BENAMIRA A., PATTANAIK S.: Application of the transfer matrix method to anti-reflective coating rendering. In *Computer Graphics International Conference, CGI, Proceedings* (2020), Springer, pp. 83–95. 3

[Bru84] BRUS L. E.: Electron–electron and electron-hole interactions in small semiconductor crystallites: The size dependence of the lowest excited electronic state. *The Journal of Chemical Physics 80*, 9 (1984), 4403–4409. 2

[Bru86] BRUS L.: Electronic wave functions in semiconductor clusters: experiment and theory. *The Journal of Physical Chemistry 90*, 12 (1986), 2555–2560. 2

[CBTB15] CHIANG M. J.-Y., BITTERLI B., TAPPAN C., BURLEY B.: A practical and controllable hair and fur model for production path tracing. In *ACM SIGGRAPH 2015 Talks* (2015). 5

[CLZ*23] CHEN X., LIN X., ZHOU L., SUN X., LI R., CHEN M., YANG Y., HOU W., WU L., CAO W., ET AL.: Blue light-emitting diodes based on colloidal quantum dots with reduced surface-bulk coupling. *Nature Communications 14*, 1 (2023), 284. 2

[CS04] CEREZO B. E., SERON F. J.: Rendering natural waters taking fluorescence into account. *Computer Animation and Virtual Worlds 15*, 5 (2004), 471–484. 2

[CVR*19] CHIZHOV A., VASILIEV R., RUMYANTSEVA M., KRYLOV I., DROZDOV K., BATUK M., HADERMANN J., ABAKUMOV A., GASKOV A.: Light-activated sub-ppm NO2 detection by hybrid ZnO/QD nanomaterials vs. charge localization in core-shell QD. *Frontiers in Materials 6* (2019), 231. 8, 13

[CVT*10] CURTO A. G., VOLPE G., TAMINIAU T. H., KREUZER M. P., QUIDANT R., VAN HULST N. F.: Unidirectional emission of a quantum dot coupled to a nanoantenna. *Science 329*, 5994 (2010), 930–933. 6

[Dhi21] DHILLON D. S. J.: Physically based rendering of simple thin volume natural nanostructures. In *Advances in Visual Computing* (Cham, 2021), Springer International Publishing, pp. 400–413. 3

[DJ18] DUPUY J., JAKOB W.: An adaptive parameterization for efficient material acquisition and rendering. *Transactions on Graphics (Proceedings of SIGGRAPH Asia) 37*, 6 (Nov. 2018), 274:1–274:18. 7, 8, 9

[Far09] FARNOOD R.: Optical properties of paper: Theory and practice. *Pulp Pap. Fud. Res. Soc. Bury 273* (2009). 10

[GBS*16] GRIGIONI I., BERNAREGGI M., SINIBALDI G., DOZZI M. V., SELLI E.: Size-dependent performance of CdSe quantum dots in the photocatalytic evolution of hydrogen under visible light irradiation. *Applied Catalysis A: General 518* (2016), 176–180. 8, 13

[GdlG09] GALIAN R. E., DE LA GUARDIA M.: The use of quantum dots in organic chemistry. *TrAC Trends in Analytical Chemistry 28*, 3 (2009), 279–291. 2

[Gla95] GLASSNER A. S.: A model for fluorescence and phosphorescence. In *Photorealistic Rendering Techniques* (Berlin, Heidelberg, 1995), Sakas G., Müller S., Shirley P., (Eds.), Springer Berlin Heidelberg, pp. 60–70. 2

[GSMA08] GUTIERREZ D., SERON F. J., MUNOZ A., ANSON O.: Visualizing underwater ocean optics. *Computer Graphics Forum 27*, 2 (2008), 547–556. 2

[GVGRB12] GARCÍA-VALENZUELA A., GUTIÉRREZ-REYES E., BARRERA R. G.: Multiple-scattering model for the coherent reflection and transmission of light from a disordered monolayer of particles. *Journal of the Optical Society of America A 29*, 6 (2012), 1161–1179. 3

[GVHPTS13] GARCÍA-VALENZUELA A., HARO-PONIATOWSKI E., TOUDERT J., SERNA R.: Evolution of the optical reflectivity of a monolayer of nanoparticles during its growth on a dielectric thin film. *Applied Physics A 110* (2013), 757–764. 3, 6

[HFW21] HUA Q., FICHET A., WILKIE A.: A compact representation for fluorescent spectral data. In *Eurographics Symposium on Rendering* (2021). 2

[HHA*10] HULLIN M. B., HANIKA J., AJDIN B., SEIDEL H.-P., KAUTZ J., LENSCH H. P.: Acquisition and analysis of bispectral bidirectional reflectance and reradiation distribution functions. 1–7. 1, 2

[HKYM01] HIRAYAMA H., KANEDA K., YAMASHITA H., MONDEN Y.: An accurate illumination model for objects coated with multilayer films. *Computers & Graphics 25*, 3 (2001), 391–400. 3

[HTFW22] HUA Q., TÁZLAR V., FICHET A., WILKIE A.: Efficient storage and importance sampling for fluorescent reflectance. In *Computer Graphics Forum* (2022), Wiley Online Library. 2

[JA18] JARABO A., ARELLANO V.: Bidirectional rendering of vector light transport. In *Computer Graphics Forum* (2018), vol. 37, Wiley Online Library, pp. 96–105. 2

[Jak10] JAKOB W.: Mitsuba renderer, 2010. http://www.mitsuba-renderer.org. 9

[JHD20] JUNG A., HANIKA J., DACHSBACHER C.: Spectral mollification for bidirectional fluorescence. In *Computer Graphics Forum* (2020), vol. 39, Wiley Online Library, pp. 373–384. 2

[JHMD18] JUNG A., HANIKA J., MARSCHNER S., DACHSBACHER C.: A simple diffuse fluorescent BBRRDF model. In *Proceedings of the Eurographics 2018 Workshop on Material Appearance Modeling* (2018), Eurographics Association, p. 15–18. 1, 2, 10

[JWH*19] JUNG A., WILKIE A., HANIKA J., JAKOB W., DACHSBACHER C.: Wide gamut spectral upsampling with fluorescence. *Computer Graphics Forum (Proceedings of Eurographics Symposium on Rendering) 38*, 4 (Oct. 2019). 2

[Ken18] KENNARD E.: On the thermodynamics of fluorescence. *Physical Review 11*, 1 (1918), 29. 2, 4

[Lak06] LAKOWICZ J. R.: *Principles Of Fluorescence Spectroscopy*. Springer, 2006. 2

[LWMB02] LEATHERDALE C. A., WOO W.-K., MIKULEC F. V., BAWENDI M. G.: On the absorption cross section of cdse nanocrystal quantum dots. *The Journal of Physical Chemistry B 106*, 31 (2002), 7619–7622. 2, 4

[MFW18] MOJZÍK M., FICHET A., WILKIE A.: Handling fluorescence in a uni-directional spectral path tracer. In *Computer Graphics Forum* (2018), vol. 37, Wiley Online Library, pp. 77–94. 2

[NSR17] NALBACH O., SEIDEL H.-P., RITSCHEL T.: Practical capture and reproduction of phosphorescent appearance. *Computer Graphics Forum 36*, 2 (2017), 409–420. 2

[Ros13] ROSSIER R.: *Framework for printing with daylight fluorescent inks*. PhD thesis, EPFL, Switzerland, 2013. 8, 9

[SDHG16] SASIHITHLU K., DAHAN N., HUGONIN J.-P., GREFFET J.-J.: A surface-scattering model satisfying energy conservation and reciprocity. *Journal of Quantitative Spectroscopy and Radiative Transfer 171* (2016), 4–14. 3, 6

[SN04] SMITH A. M., NIE S.: Chemical analysis and cellular imaging with quantum dots. *Analyst 129*, 8 (2004), 672–677. 8, 13

[Ste57] STEPANOV B. I.: Universal relation between the absorption spectra and luminescence spectra of complex molecules. In *Doklady Akademii Nauk* (1957), vol. 112, Russian Academy of Sciences, pp. 839–841. 2

[Sun06] SUN Y.: Rendering biological iridescences with RGB-based renderers. *ACM Transactions on Graphics 25*, 1 (Jan. 2006), 100–129. 3

[SW08] SUN Y., WANG Q.: Interference shaders of thin films. In *Computer Graphics Forum* (2008), vol. 27, Wiley Online Library, pp. 1607–1631. 3

[SZS*19] SRIVASTAVA A. K., ZHANG W., SCHNEIDER J., HALPERT J. E., ROGACH A. L.: Luminescent down-conversion semiconductor quantum dots and aligned quantum rods for liquid crystal displays. *Advanced Science 6*, 22 (2019), 1901345. 4

[TGSR22] TOVSTUN S., GADOMSKA A., SPIRIN M., RAZUMOV V.: Extracting the homogeneous and inhomogeneous linewidths of colloidal quantum dots from the excitation-emission matrix. *Journal of Luminescence 252* (2022), 119420. 4

[TIS*20] TOVSTUN S. A., IVANCHIKHINA A. V., SPIRIN M. G., MARTYANOVA E. G., RAZUMOV V. F.: Studying the size-selective precipitation of colloidal quantum dots by decomposing the excitation–emission matrix. *The Journal of Chemical Physics 153*, 8 (2020), 084108. 4

[TR15] TOVSTUN S., RAZUMOV V.: Theoretical analysis of nonradiative energy transfer in nanoclusters of quasi-monodisperse colloidal quantum dots. *High Energy Chemistry 49* (2015), 352–360. 4

[VPA*22] VYNCK K., PACANOWSKI R., AGREDA A., DUFAY A., GRANIER X., LALANNE P.: The visual appearances of disordered optical metasurfaces. *Nature Materials 21*, 9 (2022), 1035–1041. 3

[VRS54] VAN ROOSBROECK W., SHOCKLEY W.: Photon-radiative recombination of electrons and holes in germanium. *Physical Review 94*, 6 (1954), 1558. 2

[WBST99] WENZEL T., BOSBACH J., STIETZ F., TRÄGER F.: In situ determination of the shape of supported silver clusters during growth. *Surface science 432*, 3 (1999), 257–264. 6

[WTP01] WILKIE A., TOBLER R. F., PURGATHOFER W.: Combined rendering of polarization and fluorescence effects. In *Rendering Techniques: Proceedings of the Eurographics Workshop* (2001), Springer, pp. 197–204. 2

[WWLP06] WILKIE A., WEIDLICH A., LARBOULETTE C., PURGATHOFER W.: A reflectance model for diffuse fluorescent surfaces. In *Proceedings of the 4th International Conference on Computer Graphics and Interactive Techniques in Australasia and Southeast Asia* (2006), p. 321–331. 1, 2

[YGC*19] YAN Y., GONG J., CHEN J., ZENG Z., HUANG W., PU K., LIU J., CHEN P.: Recent advances on graphene quantum dots: from chemistry and physics to applications. *Advanced materials 31*, 21 (2019), 1808283. 2

[YTC*23] YOU Y., TONG X., CHANNA A. I., ZHI H., CAI M., ZHAO H., XIA L., LIU G., ZHAO H., WANG Z.: High-efficiency luminescent solar concentrators based on composition-tunable eco-friendly core/shell quantum dots. *Chemical Engineering Journal 452* (2023), 139490. 2

Appendix A: Mathematical Expressions

We give here the mathematical expressions of the functions used in this paper.

$$\mathcal{G}(\lambda,\lambda_m,\delta) = \exp\left(-\frac{(\lambda-\lambda_m)^2}{\delta^2}\right) \tag{29}$$

$$\mathcal{L}(\lambda,\lambda_m,\delta) = \frac{\exp\left(-\frac{(\lambda-\lambda_m)}{\delta}\right)}{\delta\left(1+\exp\left(-\frac{(\lambda-\lambda_m)}{\delta}\right)\right)^2} \tag{30}$$

$$\Lambda(\lambda,\lambda_m,\delta) = \frac{1}{1+\exp\left(-\frac{(\lambda-\lambda_m)}{\delta}\right)} \tag{31}$$

Appendix B: Comparison with Measurements

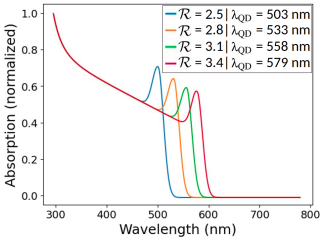

Figure 18: *Comparison between our absorption spectrum and the measured one presented in Figure 2 of Grigioni et al. work [GBS*16]. We can see that our position of the cut-off wavelength is in good agreement with the measurement, as well as the relative evolution of the Gaussian peak.*

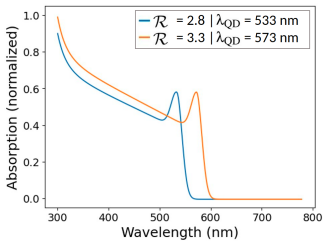

Figure 19: *Comparison between our absorption spectrum and the measured one presented in Figure 3 of Chizhov et al. work [CVR*19]. We can see that our position of the cut-off wavelength matches very well with the measurement. The last curve of the measurement represents a QD made of two different molecules which we do not model in our work.*

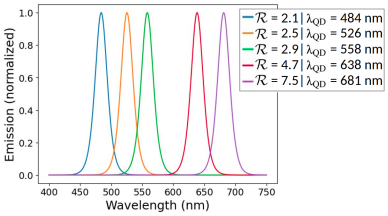

Figure 20: *Comparison between our Emission spectrum and the measured one presented in Figure 1 of Smith and Nie's work [SN04]. We reproduce the curves in blue, green, yellow, light red and dark red as they were the only ones provided with a value of the QD radius. We can see that the center and the width of the modeled emission spectrum match the measurements very well.*

We qualitatively compare the absorption and emission spectra derived from our model to the measured data presented in [GBS*16, CVR*19, SN04]. It is important to notice that it is the general shape and position of the absorption peak around the cut-off wavelength that is key to compare. The exact value of the absorption depends on the concentration of the solution. We see that our model conserves the main elements of the QD behavior: (i) High absorption in UV; (ii) A cut-off wavelength which increases with the radius of the QD; (iii) A Gaussian profile around the cut-off wavelength; (iv) A Gaussian emission spectrum centered on a wavelength which increases with the radius $\mathcal{R}$ of the QD.

We can see that overall, the shape of the spectrum and the position of the cut-off wavelength obtained with our model is in very good agreement with the absorbance curves obtained from physical measurements. The principal discrepancies appear in the shorter wavelength range of the absorption spectrum. Indeed, as stated earlier, our model assumes that the permittivity of the QD is independent of its size, which explains that the portions of the absorption curves at low wavelengths are superposed, regardless of the QD radius.